



Observation of the decay $B_s^0 \rightarrow \bar{D}^0\phi^\star$

LHCb Collaboration

ARTICLE INFO

Article history:

Received 23 August 2013

Received in revised form 10 October 2013

Accepted 25 October 2013

Available online 31 October 2013

Editor: L. Rolandi

ABSTRACT

First observation of the decay $B_s^0 \rightarrow \bar{D}^0\phi$ is reported using pp collision data, corresponding to an integrated luminosity of 1.0 fb^{-1} , collected by the LHCb experiment at a centre-of-mass energy of 7 TeV . The significance of the signal is 6.5 standard deviations. The branching fraction is measured relative to that of the decay $B_s^0 \rightarrow \bar{D}^0\bar{K}^{*0}$ to be

$$\frac{\mathcal{B}(B_s^0 \rightarrow \bar{D}^0\phi)}{\mathcal{B}(B_s^0 \rightarrow \bar{D}^0\bar{K}^{*0})} = 0.069 \pm 0.013 \text{ (stat)} \pm 0.007 \text{ (syst).}$$

The first measurement of the ratio of branching fractions for the decays $B_s^0 \rightarrow \bar{D}^0\bar{K}^{*0}$ and $B^0 \rightarrow \bar{D}^0K^{*0}$ is found to be

$$\frac{\mathcal{B}(B_s^0 \rightarrow \bar{D}^0\bar{K}^{*0})}{\mathcal{B}(B^0 \rightarrow \bar{D}^0K^{*0})} = 7.8 \pm 0.7 \text{ (stat)} \pm 0.3 \text{ (syst)} \pm 0.6 \text{ (} f_s/f_d \text{)},$$

where the last uncertainty is due to the ratio of the B_s^0 and B^0 fragmentation fractions.

© 2013 CERN. Published by Elsevier B.V. All rights reserved.



1. Introduction

Measurements of the decay¹ $B_s^0 \rightarrow \bar{D}^0\phi$ are of particular interest because they provide information that can be used to determine the CKM angles $\gamma \equiv \arg[-V_{ud}V_{ub}^*/(V_{cd}V_{cb}^*)]$ and $\beta_s \equiv \arg[-V_{ts}V_{tb}^*/(V_{cs}V_{cb}^*)]$ without theoretical uncertainties [1]. Knowledge of these CP -violating phases is crucial to search for new sources of CP violation and unravel subtle effects of physics beyond the Standard Model, which may appear in flavour-changing interactions. Their precise measurements are among the most important goals of flavour physics experiments.

To date, the angle γ is the least well-determined angle of the Unitarity Triangle with an uncertainty of about 10° [2–4]. The current precision is dominated by measurements of time-integrated $B^+ \rightarrow DK^+$ decay rates, where D indicates a superposition of D^0 and \bar{D}^0 decays to a common final state. In these decays, sensitivity to γ arises from direct CP violation in the interference between the $b \rightarrow c\bar{s}$ and $b \rightarrow u\bar{c}s$ tree-level amplitudes. As there are no loop contributions to the decay amplitudes, no theoretical uncertainties arise. The main limitation is due to the size of the data samples collected by the experiments. To improve on the precision, it is important to perform additional measurements from other channels with small theoretical uncertainties.

The large production cross-section of B_s^0 mesons in pp collisions at the LHC opens new possibilities for measuring both γ and β_s . For example, the decay $B_s^0 \rightarrow D_s^\pm K^\mp$ is sensitive to $\gamma + 2\beta_s$ through measurements of time-dependent decay rates [5,6]; although the determination of γ from this mode requires an independent measurement of the mixing phase β_s .

The decay $B_s^0 \rightarrow \bar{D}^0\phi$, first proposed in 1991 by Gronau and London for measuring γ [7], can also probe β_s via measurements of time-dependent decay rates. Nandi and London have shown [1] that both γ and β_s can be determined without theoretical uncertainties and ambiguities, using the known sign of $\Delta\Gamma_s$, the decay-width difference between the two B_s^0 mass eigenstates [8].

An alternative method to measure γ using $B_s^0 \rightarrow D\phi$ decays was proposed in Refs. [9,10], where it was shown that γ can be determined from time-integrated decay rates, in a similar way as from $B^+ \rightarrow DK^+$ decays, even if $B_s^0 \rightarrow D\phi$ is not a self-tagged decay mode. The only requirement for the determination is that a sufficient number of different D final states are included in the measurement. The time-integrated method does not require flavour-tagging, and hence makes optimal use of the statistical power of the large $b\bar{b}$ production at LHC. An estimation of the sensitivity with this method shows that the mode $B_s^0 \rightarrow D\phi$ has the potential to make a significant impact on the determination of γ at LHCb [11].

The observation of the $B_s^0 \rightarrow \bar{D}^0\phi$ decay and the measurement of its branching fraction, described in this Letter, are the first steps towards a programme of CP violation studies with this channel. The branching fraction is measured relative to the

[☆] © CERN for the benefit of the LHCb Collaboration.

¹ The inclusion of charge conjugate processes is implied, unless otherwise stated.

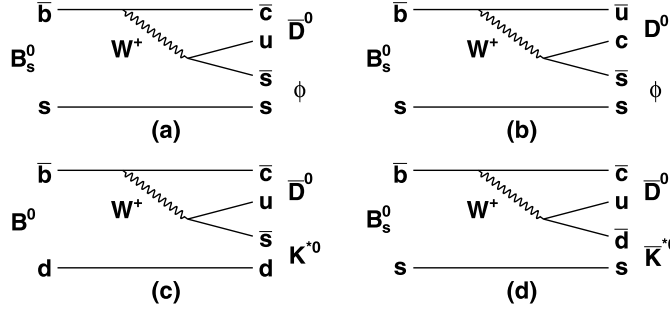


Fig. 1. Feynman diagrams for the following decays: (a) $B_s^0 \rightarrow \bar{D}^0 \phi$; (b) $B_s^0 \rightarrow D^0 \phi$; (c) $B^0 \rightarrow \bar{D}^0 K^{*0}$, and (d) $B_s^0 \rightarrow \bar{D}^0 K^{*0}$. The $B_s^0 \rightarrow \bar{D}^0 \phi$ and $B_s^0 \rightarrow D^0 \phi$ decay amplitudes interfere when \bar{D}^0 and D^0 decay to the same final state.

topologically similar decay $B_s^0 \rightarrow \bar{D}^0 \bar{K}^{*0}$, that was previously observed by LHCb [12]. In addition, the first measurement of the branching fraction of the $B_s^0 \rightarrow \bar{D}^0 \bar{K}^{*0}$ decay relative to the $B^0 \rightarrow \bar{D}^0 K^{*0}$ decay is reported and used to improve on the knowledge of the branching fraction of the $B_s^0 \rightarrow \bar{D}^0 \bar{K}^{*0}$ decay. The Feynman diagrams corresponding to the $B_s^0 \rightarrow \bar{D}^0 \phi$ and $B_s^0 \rightarrow D^0 \phi$ decay amplitudes are shown in Fig. 1. The Feynman diagrams for the leading $b \rightarrow c$ amplitudes in $B_s^0 \rightarrow \bar{D}^0 \bar{K}^{*0}$ and $B^0 \rightarrow \bar{D}^0 K^{*0}$ decays are also shown in Fig. 1. Since only $D^0 \rightarrow K^- \pi^+$ decays are considered in this study, all of the measured quantities for the $B_s^0 \rightarrow \bar{D}^0 \phi$, $B_s^0 \rightarrow \bar{D}^0 \bar{K}^{*0}$, and $B^0 \rightarrow \bar{D}^0 K^{*0}$ channels include contributions from the $B_s^0 \rightarrow D^0 \phi$, $B_s^0 \rightarrow D^0 \bar{K}^{*0}$, and $B^0 \rightarrow D^0 K^{*0}$ modes, respectively, through the doubly-Cabibbo-suppressed decay $D^0 \rightarrow K^+ \pi^-$.

2. Event selection

The study reported here is based on pp collision data, corresponding to an integrated luminosity of 1.0 fb^{-1} , collected by the LHCb experiment at a centre-of-mass energy of 7 TeV . The LHCb detector [13] is a single-arm forward spectrometer covering the pseudorapidity range $2 < \eta < 5$, designed for the study of particles containing b or c quarks. The detector includes a high-precision tracking system consisting of a silicon-strip vertex detector surrounding the pp interaction region, a large-area silicon-strip detector located upstream of a dipole magnet with a bending power of about 4 Tm , and three stations of silicon-strip detectors and straw drift tubes placed downstream. The combined tracking system provides a momentum (p) measurement with relative uncertainty that varies from 0.4% at $5 \text{ GeV}/c$ to 0.6% at $100 \text{ GeV}/c$, and impact parameter (IP) resolution of $20 \mu\text{m}$ for tracks with large transverse momentum (p_T). Charged hadrons are identified using two ring-imaging Cherenkov detectors [14]. Photon, electron and hadron candidates are identified by a calorimeter system consisting of scintillating-pad and preshower detectors, an electromagnetic calorimeter and a hadronic calorimeter. Muons are identified by a system composed of alternating layers of iron and multiwire proportional chambers [15]. The trigger [16] consists of a hardware stage, based on information from the calorimeter and muon systems, followed by a software stage, which applies a full event reconstruction.

Simulated signal samples and data control channels are used to optimise the selection criteria. In the simulation, pp collisions are generated using PYTHIA 6.4 [17] with a specific LHCb configuration [18]. Decays of hadrons are described by EvtGEN [19], in which final state radiation is generated using PHOTOS [20]. The interaction of the generated particles with the detector and its response are implemented using the GEANT4 toolkit [21] as described in Ref. [22].

Selected events fulfill one of two hardware trigger requirements: either a particle from the signal decay deposits enough

energy in the calorimeter system, or one of the particles in the event, not originating from the signal decay, fulfils any of the trigger requirements (e.g., events triggered by one or more particles coming from the decay of the other B meson in the $pp \rightarrow bbX$ event). The software trigger requires a two-, three- or four-track secondary vertex with a large scalar sum of the tracks p_T and significant displacement from the associated primary pp interaction vertex (PV). At least one track should have $p_T > 1.7 \text{ GeV}/c$ and a value of $\chi_{\text{IP}}^2 > 16$, where χ_{IP}^2 is defined as the difference between the χ^2 of the PV reconstructed with and without the considered particle. A multivariate algorithm identifies secondary vertices consistent with the decay of a b hadron.

Reconstructed tracks are selected with criteria on their p , p_T , track χ^2 per degree of freedom, χ_{IP}^2 and particle identification (PID). Tracks identified as muons are discarded.

The D^0 mesons are reconstructed in the decay mode $D^0 \rightarrow K^- \pi^+$. Particle identification criteria used to select the daughters require the difference between the log-likelihoods of the kaon and pion hypotheses ($\Delta LL_{K\pi}$) to be larger than 0 for the kaon and smaller than 4 for the pion. The D^0 meson χ_{IP}^2 is required to be larger than 2 to separate mesons originating from a B decay and those produced at the PV. In addition, for the $\bar{D}^0 K^{*0}$ ($\bar{D}^0 \bar{K}^{*0}$) final states, the charm meson flight distance with respect to the $B_{(s)}^0$ vertex is required to be larger than 0 with a significance of at least 2 standard deviations in order to suppress background from $B_{(s)}^0$ decays without an intermediate charm meson, such as the mode $B^0 \rightarrow K^- \pi^+ K^{*0}$. There is no corresponding requirement in the $\bar{D}^0 \phi$ final state, since the charmless background is negligible. The D^0 candidates with invariant mass within $\pm 20 \text{ MeV}/c^2$ of the known mass [23] are retained.

The ϕ mesons are reconstructed in the mode $\phi \rightarrow K^+ K^-$. The p_T of the kaon daughters is required to be larger than $350 \text{ MeV}/c$ and the $\Delta LL_{K\pi}$ of both daughters to be larger than 3. Candidates are retained if their invariant mass is within $\pm 10 \text{ MeV}/c^2$ of the known ϕ mass [23].

The K^{*0} mesons are reconstructed in the mode $K^{*0} \rightarrow K^+ \pi^-$. The p_T of the kaon (pion) is required to be larger than 350 (250) MeV/c . In addition, to reduce the cross-feed from $B^0 \rightarrow \bar{D}^0 \rho^0$ and $B^0 \rightarrow \bar{D}^0 K^+ K^-$ decays, the $\Delta LL_{K\pi}$ of the kaon must be larger than 3 and that of the pion smaller than 3. Possible background from protons in the kaon sample, for example from the decay $A_b^0 \rightarrow D^0 p \pi^-$, is suppressed by selecting kaon candidates with a difference between the log-likelihoods of proton and kaon hypotheses, ΔLL_{pK} , smaller than 10. Candidate K^{*0} mesons with invariant mass within $\pm 50 \text{ MeV}/c^2$ of the known mass [23] are kept.

Neutral B meson candidates are formed from \bar{D}^0 and ϕ ($\text{or } K^{*0}$) candidates, which are fitted to a common vertex with the \bar{D}^0 constrained to its known mass. In order to reduce contributions from non-resonant decays, $B_{(s)}^0 \rightarrow \bar{D}^0 K^+ K^-$, $B_s^0 \rightarrow \bar{D}^0 K^- \pi^+$, and

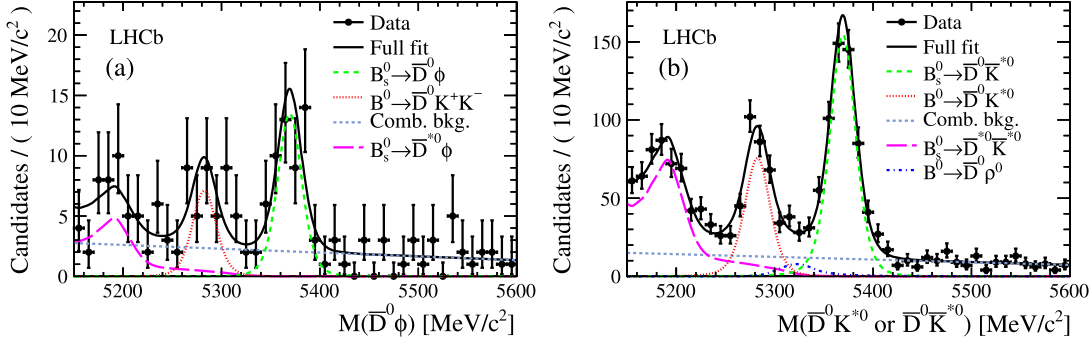


Fig. 2. Invariant mass distributions for (a) $B_s^0 \rightarrow \bar{D}^0\phi$, and (b) $B^0 \rightarrow \bar{D}^0K^{*0}$ or $B_s^0 \rightarrow \bar{D}^0\bar{K}^{*0}$ decays. Data points are shown in black, the total fitted PDF as solid black line, and the components as detailed in the legends.

$B^0 \rightarrow \bar{D}^0K^+\pi^-$ [24,25], the absolute value of the cosine of the vector-daughter helicity angle ($\cos\theta_h$) is required to be larger than 0.4. This angle is defined between the momentum direction of the K^+ daughter in the ϕ (K^{*0}) frame, and the vector meson direction in the B rest frame. Backgrounds from $B_{(s)}^0 \rightarrow D_{(s)}^\mp h^\pm$ ($h = \pi, K$) decays, are rejected by vetoing candidates with $K^+K^-\pi^+$ ($K^-\pi^+\pi^+$ and $K^+K^-\pi^+$) invariant mass within ± 15 MeV/ c^2 of the D_s^+ (D^+) meson known mass [23].

A boosted decision tree (BDT) [26] suppresses the residual background. Nine variables are input to the BDT: the decay vertex χ^2 of the reconstructed $B_{(s)}^0$ and D^0 mesons; the χ^2_{IP} of the $B_{(s)}^0$, D^0 , ϕ (K^{*0}) mesons, and of both the D^0 daughters; and the p_T of the D^0 and ϕ (K^{*0}) mesons. The BDT is optimised and tested using simulated signal events and events outside of the D^0 mass signal region for background. Events with BDT response larger than 0.2 are retained, resulting in a rejection of 74% of the background, while retaining 84% of the signal. The working point maximises $N_s/\sqrt{N_s + N_b}$. Here, N_s is the expected $B_s^0 \rightarrow \bar{D}^0\phi$ signal yield, computed using simulated events and assuming that the branching fraction is equal to that of the $B^0 \rightarrow \bar{D}^0K^{*0}$ decay (as expected under SU(3) flavour symmetry), and N_b is the background yield estimated using data events in the sidebands outside the $B_s^0 \rightarrow \bar{D}^0\phi$ signal region (± 50 MeV/ c^2 around the B_s^0 known mass [23]). No multiple candidates are found for the $\bar{D}^0\phi$ final state. The fraction of events with more than one candidate is 0.6% in the $\bar{D}^0\bar{K}^{*0}$ or \bar{D}^0K^{*0} invariant mass range of 5150–5600 MeV/ c^2 , and the candidate retained is chosen randomly.

3. Signal yield

Signal yields are determined with an unbinned maximum likelihood fit to the $\bar{D}^0\phi$ and the sum of the \bar{D}^0K^{*0} and $\bar{D}^0\bar{K}^{*0}$ invariant mass (M) distributions in the range $5150 < M < 5600$ MeV/ c^2 . The two samples are fitted simultaneously with a sum of probability density functions (PDFs) modelling signal and background contributions.

The B_s^0 and B^0 signals are described by a modified Gaussian distribution of the form

$$f(M; \mu, \sigma, \alpha_L, \alpha_R) \propto \exp\left(\frac{-(M - \mu)^2}{2\sigma^2 + \alpha_{L,R}(M - \mu)^2}\right), \quad (1)$$

where μ is the peak position, σ the width, and α_L ($M < \mu$) and α_R ($M > \mu$) parameterise the tails. The width and the tail parameters depend on the final state, but are common to the B_s^0 and B^0 decays. The B^0 peak position and width are left free to vary in the fit with the difference between B_s^0 and B^0 peak positions fixed to the current world-average value [23]. The tail parameters are fixed to values determined from simulated events and

are considered among the sources of systematic uncertainty. The recently observed decay $B^0 \rightarrow \bar{D}^0K^+K^-$ [24] is expected to contribute to the $\bar{D}^0\phi$ distribution and is modelled with the same modified Gaussian distribution, but with different peak position, as that used to describe the $B_s^0 \rightarrow \bar{D}^0\phi$ decay.

Background from the $B^0 \rightarrow \bar{D}^0\rho^0$ decay in the \bar{D}^0K^{*0} (or $\bar{D}^0\bar{K}^{*0}$) final state can arise from misidentification of one of the pions from the $\rho^0 \rightarrow \pi^+\pi^-$ decay as a kaon. The shape of this cross-feed contribution is modelled with a Crystal Ball function [27] determined from simulated events. This background component is absent in the $B_s^0 \rightarrow \bar{D}^0\phi$ mode, since the probability that both pions are misidentified as kaons and that their invariant mass is inside the narrow ϕ mass window is negligible. For similar reasons, the cross-feed between $B^0 \rightarrow \bar{D}^0K^{*0}$ and $B_s^0 \rightarrow \bar{D}^0\phi$ decays is negligible.

The decay $B_s^0 \rightarrow \bar{D}^{*0}\bar{K}^{*0}$, where a π^0 or photon from the \bar{D}^{*0} decay is not reconstructed, constitutes the main background contribution to the $\bar{D}^0\bar{K}^{*0}$ final state below the B^0 mass. Similarly, the decay $B_s^0 \rightarrow \bar{D}^{*0}\phi$ is expected to contribute to the low-mass background in the $\bar{D}^0\phi$ final state. These decays of a pseudoscalar to two vector mesons are modelled by a non-parametric PDF [28] determined from simulation. The mass shape depends on the unknown fraction of longitudinal polarisation, which is assumed to be identical for the two modes and is treated as an additional free parameter in the fit.

The remaining combinatorial background is described by a linear function, with a common slope for the two considered final states, left free to vary in the fit.

Signal yield ratios are directly determined in the fit to take into account statistical correlations in the measurement of ratios of branching fractions. In total, there are 13 free parameters in the fit, including the background yields of the different components and the overall normalisation. The invariant mass distributions with the resulting fits are shown in Fig. 2.

The helicity angle distribution of the ϕ candidates for the B_s^0 and B^0 signal is investigated. The *sPlot* [29] technique is adopted to assign a weight to the events and determine the signal components, using the $\bar{D}^0\phi$ invariant mass as the discriminating variable. For this purpose, the requirement on $\cos\theta_h > 0.4$ has been lifted prior to the computation of the signal weights. The data distributions of $\cos\theta_h$, shown in Fig. 3, are compared to the expected distribution of $B_s^0 \rightarrow \bar{D}^0\phi$ decays from simulation. The distribution observed for the $B^0 \rightarrow \bar{D}^0K^+K^-$ decay candidates is consistent with the expectation that this decay is not dominated by a pseudoscalar-vector quasi-two-body final state.

The signal yield ratios are corrected for two residual backgrounds that peak at the mass of the B_s^0 or B^0 meson and are distributed as the signal. The first of the two backgrounds is the

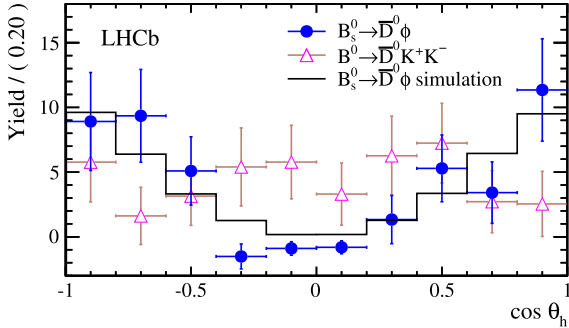


Fig. 3. Distribution of the cosine of the helicity angle of the ϕ candidates.

Uncorrected signal yields and the peaking (charmless, S-wave) background yields.			
Channel	Signal	Charmless background	S-wave background
$B_s^0 \rightarrow \bar{D}^0\phi$	43 ± 8	0 ± 2	2 ± 3
$B_s^0 \rightarrow \bar{D}^0\bar{K}^{*0}$	535 ± 30	4 ± 3	24 ± 7
$B^0 \rightarrow \bar{D}^0K^{*0}$	260 ± 24	4 ± 3	13 ± 6

charmless background due to the decays $B_s^0 \rightarrow K^+\pi^-\bar{K}^{*0}$ and $B^0 \rightarrow K^+\pi^-\bar{K}^{*0}$ proceeding without the presence of an intermediate \bar{D}^0 meson. There is no evidence of such background in the $B_s \rightarrow \bar{D}^0\phi$ channel. A large fraction of the charmless background in the \bar{D}^0K^{*0} final state is rejected with the requirement of a minimal D^0 flight distance introduced in Section 2. The remaining charmless background is evaluated using candidates from the D^0 sidebands. The B yields in the D^0 sidebands above a linear background are extrapolated to the D^0 signal region and used to correct the signal. The uncorrected signal yields and the background contributions are given in Table 1. The other source of peaking background is due to higher mass resonances and non-resonant $B_s^0 \rightarrow \bar{D}^0K^+K^-$, $B_s^0 \rightarrow \bar{D}^0K^-\pi^+$, and $B^0 \rightarrow \bar{D}^0K^+\pi^-$ decays that fall in the $B_s^0 \rightarrow \bar{D}^0\phi$, $B_s^0 \rightarrow \bar{D}^0\bar{K}^{*0}$, and $B^0 \rightarrow \bar{D}^0K^{*0}$ signal regions, respectively. This contribution is evaluated with fits to the ϕ and K^{*0} background-subtracted mass distributions in a wider range than the signal window. The background subtraction is performed using the *sPlot* technique, with the $\bar{D}^0\phi$ and $\bar{D}^0\bar{K}^{*0}$ (or \bar{D}^0K^{*0}) mass as discriminating variables. A linear PDF describes the S-wave background in the $\bar{D}^0\phi$ final state. A spin-one Breit–Wigner distribution convolved with a Gaussian resolution function describes the signal, and an S-wave PDF the non-resonant background. The S-wave component in the $B^0 \rightarrow \bar{D}^0K^{*0}$ and $B_s^0 \rightarrow \bar{D}^0\bar{K}^{*0}$ channels takes into account non-resonant and $K^{*0}(1430)$ resonance contributions and uses experimental input from the LASS experiment [30]. It is approximately linear in the region of interest, ± 200 MeV/c 2 around the K^{*0} nominal mass. Potential interference effects between the S-wave and the P-wave components are covered by the assigned systematic uncertainty. The ϕ and \bar{K}^{*0} mass distributions are shown in Fig. 4. The background yields, after extrapolation to the K^{*0} and ϕ signal mass windows, are listed in Table 1.

A likelihood ratio test is employed to assess the statistical significance of the $B_s^0 \rightarrow \bar{D}^0\phi$ signal, which is given by $\sqrt{2\ln(\mathcal{L}_{s+b}/\mathcal{L}_b)}$ and found to be 7.1 standard deviations. Here \mathcal{L}_{s+b} and \mathcal{L}_b are the maximum values of the likelihoods for the signal-plus-background and background-only hypotheses, respectively.

The ratios of branching fractions are evaluated from the uncorrected signal yields, N , and the sum of the charmless and non-resonant background yields, N^{bkg} , as

$$\begin{aligned} \mathcal{R}_\phi &\equiv \frac{\mathcal{B}(B_s^0 \rightarrow \bar{D}^0\phi)}{\mathcal{B}(B_s^0 \rightarrow \bar{D}^0\bar{K}^{*0})} \\ &= \frac{N_{B_s^0 \rightarrow \bar{D}^0\phi}}{N_{B_s^0 \rightarrow \bar{D}^0\bar{K}^{*0}}} \cdot \frac{\left(1 - \frac{N_{B_s^0 \rightarrow \bar{D}^0\phi}}{N_{B_s^0 \rightarrow \bar{D}^0\phi}}\right)}{\left(1 - \frac{N_{B_s^0 \rightarrow \bar{D}^0\bar{K}^{*0}}}{N_{B_s^0 \rightarrow \bar{D}^0\bar{K}^{*0}}}\right)} \cdot \frac{\epsilon_{B_s^0 \rightarrow \bar{D}^0\bar{K}^{*0}}}{\epsilon_{B_s^0 \rightarrow \bar{D}^0\phi}} \\ &\cdot \frac{\mathcal{B}(K^{*0} \rightarrow K^+\pi^-)}{\mathcal{B}(\phi \rightarrow K^+K^-)}, \end{aligned} \quad (2)$$

and

$$\begin{aligned} \mathcal{R}_{K^{*0}} &\equiv \frac{\mathcal{B}(B_s^0 \rightarrow \bar{D}^0\bar{K}^{*0})}{\mathcal{B}(B^0 \rightarrow \bar{D}^0K^{*0})} \\ &= \frac{N_{B_s^0 \rightarrow \bar{D}^0\bar{K}^{*0}}}{N_{B^0 \rightarrow \bar{D}^0K^{*0}}} \cdot \frac{\left(1 - \frac{N_{B_s^0 \rightarrow \bar{D}^0\bar{K}^{*0}}}{N_{B_s^0 \rightarrow \bar{D}^0\bar{K}^{*0}}}\right)}{\left(1 - \frac{N_{B^0 \rightarrow \bar{D}^0K^{*0}}}{N_{B^0 \rightarrow \bar{D}^0K^{*0}}}\right)} \\ &\cdot \frac{\epsilon_{B^0 \rightarrow \bar{D}^0K^{*0}}}{\epsilon_{B_s^0 \rightarrow \bar{D}^0\bar{K}^{*0}}} \cdot \left(\frac{f_s}{f_d}\right)^{-1}, \end{aligned} \quad (3)$$

where the ratio of the B_s^0 and B^0 fragmentation fractions is $f_s/f_d = 0.256 \pm 0.020$ [31], the value of the $\phi \rightarrow K^+K^-$ branching fraction is 0.489 ± 0.005 [23], and $\mathcal{B}(K^{*0} \rightarrow K^+\pi^-) = 2/3$. The total efficiencies, ϵ , account for the geometrical acceptance of the detector, the reconstruction, the event selection, the PID, and the trigger efficiencies. All efficiencies are computed from simulated events, except for the PID and hardware trigger efficiencies, which are obtained from data, using a high-purity calibration sample of $D^{*+} \rightarrow D^0(\rightarrow K^-\pi^+)\pi^+$ decays. The resulting ratios of branching fractions are $\mathcal{R}_\phi = 0.069 \pm 0.013$ and $\mathcal{R}_{K^{*0}} = 7.8 \pm 0.7$, where the uncertainties are statistical only.

4. Systematic uncertainties

Several sources of systematic uncertainties are considered. Those associated to the trigger and PID selection affect only \mathcal{R}_ϕ and are mainly due to systematic uncertainties in the calibration procedure. The ratios of the efficiencies of the decays $B_s^0 \rightarrow \bar{D}^0\phi$ and $B_s^0 \rightarrow \bar{D}^0\bar{K}^{*0}$ for the trigger and PID are found to be 0.97 ± 0.05 and 1.08 ± 0.03 , respectively, where the errors are propagated as systematic uncertainties to \mathcal{R}_ϕ .

Similarly, the uncertainty on the efficiencies of the charm meson flight distance selection affects only \mathcal{R}_ϕ , where different criteria are chosen for the $B_s^0 \rightarrow \bar{D}^0\phi$ and $B_s^0 \rightarrow \bar{D}^0\bar{K}^{*0}$ modes. The ratio of the corresponding efficiencies is found to be 1.27 ± 0.03 , where the uncertainty includes a contribution from the difference between data and simulation. In order to estimate the efficiency in data, the fit to the invariant mass of the B candidates is performed to data samples selected with all criteria except that on the flight distance. For this sample, the charmless background contribution is estimated using events in the upper D mass sideband and subtracted from the signal yields.

The ratio of the efficiencies for the decays $B_s^0 \rightarrow \bar{D}^0\phi$ and $B_s^0 \rightarrow \bar{D}^0\bar{K}^{*0}$ of the remaining selection criteria is found to be 1.21 ± 0.03 , where the deviation from unity is mainly due to the different widths and mass windows for the ϕ and K^{*0} resonances. The ratio of the efficiencies for the decays $B_s^0 \rightarrow \bar{D}^0\bar{K}^{*0}$ and $B^0 \rightarrow \bar{D}^0K^{*0}$ is found from simulation to be 1.04 ± 0.01 . The uncertainties on these efficiencies are propagated as systematic uncertainties due to the selection.

The fit procedure is validated using simulated pseudo-experiments. The fit bias, relative to the fitted ratio, is evaluated to be

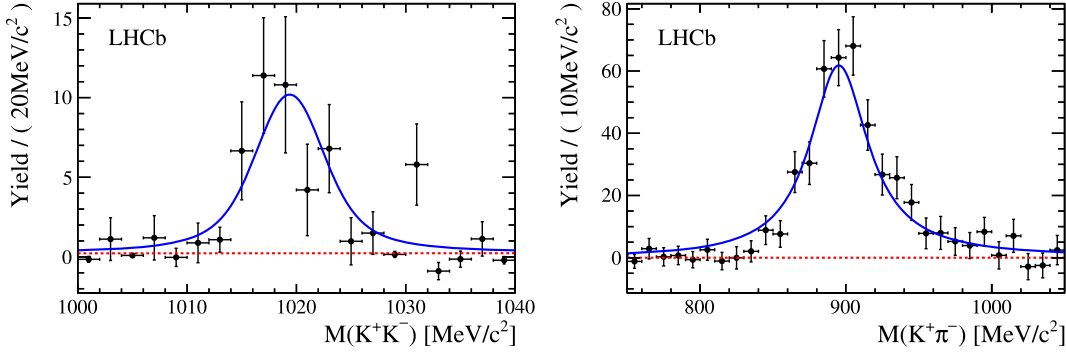


Fig. 4. Background-subtracted distributions of the reconstructed (left) ϕ mass from the $B_s^0 \rightarrow \bar{D}^0\phi$ decay and (right) \bar{K}^{*0} mass from the $B_s^0 \rightarrow \bar{D}^0\bar{K}^{*0}$ decay. The dashed red line represents the S-wave component, the solid blue line the total fit result.

Table 2

Absolute systematic uncertainties of the measured ratio of branching fractions. The total is obtained as sum in quadrature of the different contributions.

Source	\mathcal{R}_ϕ	$\mathcal{R}_{K^{*0}}$
Trigger	0.003	–
PID	0.002	–
Flight distance	0.002	–
Selection	0.002	–
Simulation statistics	0.001	0.10
Fit bias	0.001	0.03
Signal model	0.001	0.04
Background model	0.001	0.01
Charmless correction	0.003	0.10
Non-resonant correction	0.004	0.22
ϕ branching fraction	0.001	–
Total	0.007	0.26

1.4% for \mathcal{R}_ϕ and 0.2% for $\mathcal{R}_{K^{*0}}$ and is assigned as systematic uncertainty. The signal model uncertainty is evaluated by varying the fixed signal parameters by 10%, which is about three times the difference between data and simulation, as determined by a fit where those parameters are free to vary. The background shape uncertainty is determined from the bias in the results obtained by fitting samples generated with an alternative (exponential) combinatorial background model.

The uncertainties on the charmless background yields given in Table 1 are assumed to be uncorrelated and are propagated to assign the associated systematic uncertainty. Similarly, the statistical uncertainties on the S-wave background yields are propagated to \mathcal{R}_ϕ and $\mathcal{R}_{K^{*0}}$ to assign respective systematic uncertainties due to the non-resonant correction.

A summary of the systematic uncertainties is given in Table 2. The uncertainty on the fragmentation fraction f_s/f_d , which is the dominant systematic uncertainty for $\mathcal{R}_{K^{*0}}$, is not included, and is listed separately.

5. Results and conclusions

The significance of the $B_s^0 \rightarrow \bar{D}^0\phi$ signal, including systematic uncertainties, is obtained by scaling the statistical significance with the ratio of the statistical to the total (statistical and systematic) uncertainty on the signal yield. It is found to be 6.5 standard deviations. This decay is therefore observed for the first time.

The ratios of branching fractions are found to be

$$\mathcal{R}_\phi = 0.069 \pm 0.013 \text{ (stat)} \pm 0.007 \text{ (syst)},$$

$$\mathcal{R}_{K^{*0}} = 7.8 \pm 0.7 \text{ (stat)} \pm 0.3 \text{ (syst)} \pm 0.6 \text{ } (f_s/f_d).$$

From $\mathcal{R}_{K^{*0}}$ and the value of the $B^0 \rightarrow \bar{D}^0 K^{*0}$ branching fraction from Ref. [23], the $B_s^0 \rightarrow \bar{D}^0 \bar{K}^{*0}$ branching fraction is calculated to be

$$\mathcal{B}(B_s^0 \rightarrow \bar{D}^0 \bar{K}^{*0}) = [3.3 \pm 0.3 \text{ (stat)} \pm 0.1 \text{ (syst)} \pm 0.3 \text{ } (f_s/f_d) \\ \pm 0.5 \text{ } (\mathcal{B}(B^0 \rightarrow \bar{D}^0 K^{*0}))] \times 10^{-4}.$$

This result is consistent with and improves on the previous determination by LHCb [12], which is based on an independent data sample. Using the above results for \mathcal{R}_ϕ , $\mathcal{R}_{K^{*0}}$ and the $B^0 \rightarrow \bar{D}^0 K^{*0}$ branching fraction, the branching fraction for $B_s^0 \rightarrow \bar{D}^0 \phi$ is calculated to be

$$\mathcal{B}(B_s^0 \rightarrow \bar{D}^0 \phi) = [2.3 \pm 0.4 \text{ (stat)} \pm 0.2 \text{ (syst)} \pm 0.2 \text{ } (f_s/f_d) \\ \pm 0.3 \text{ } (\mathcal{B}(B^0 \rightarrow \bar{D}^0 K^{*0}))] \times 10^{-5},$$

which takes into account the correlation in the statistical uncertainties between \mathcal{R}_ϕ and $\mathcal{R}_{K^{*0}}$ of -13.6% . The correlation between the corresponding systematic uncertainties is negligible. The central value is about a factor two smaller than the branching fraction for the $B^0 \rightarrow \bar{D}^0 K^{*0}$ decay and supports the observation of SU(3) breaking effects in other colour suppressed $B_{(s)}^0 \rightarrow \bar{D}^0 V$ decays [12], where V is a vector meson. With larger data samples, the $B_s^0 \rightarrow \bar{D}^0 \phi$ decay will contribute to the measurements of the CP violating phases γ and β_s .

Acknowledgements

We express our gratitude to our colleagues in the CERN accelerator departments for the excellent performance of the LHC. We thank the technical and administrative staff at the LHCb institutes. We acknowledge support from CERN and from the national agencies: CAPES, CNPq, FAPERJ and FINEP (Brazil); NSFC (China); CNRS/IN2P3 and Region Auvergne (France); BMBF, DFG, HGF and MPG (Germany); SFI (Ireland); INFN (Italy); FOM and NWO (The Netherlands); SCSR (Poland); MEN/IFA (Romania); MinES, Rosatom, RFBR and NRC “Kurchatov Institute” (Russia); MinECo, XuntaGal and GENCAT (Spain); SNSF and SER (Switzerland); NAS Ukraine (Ukraine); STFC (United Kingdom); NSF (USA). We also acknowledge the support received from the ERC under FP7. The Tier1 computing centres are supported by IN2P3 (France), KIT and BMBF (Germany), INFN (Italy), NWO and SURF (The Netherlands), PIC (Spain), GridPP (United Kingdom). We are thankful for the computing resources put at our disposal by Yandex LLC (Russia), as well as to the communities behind the multiple open source software packages that we depend on.

Open access

This article is published Open Access at sciedirect.com. It is distributed under the terms of the Creative Commons Attribution License 3.0, which permits unrestricted use, distribution, and reproduction in any medium, provided the original authors and source are credited.

References

- [1] S. Nandi, D. London, $B_s^0(\bar{B}_s^0) \rightarrow D_{CP}^0 K\bar{K}$: Detecting and discriminating new physics in $B_s^0-\bar{B}_s^0$ mixing, Phys. Rev. D 85 (2012) 114015, arXiv:1108.5769 [hep-ph].
- [2] BaBar Collaboration, J. Lees, et al., Observation of direct CP violation in the measurement of the Cabibbo–Kobayashi–Maskawa angle γ with $B^\pm \rightarrow D^{(*)} K^{(*)\pm}$ decays, Phys. Rev. D 87 (2013) 052015, arXiv:1301.1029.
- [3] Belle Collaboration, K. Trabelsi, Study of direct CP in charmed B decays and measurement of the CKM angle γ at Belle, arXiv:1301.2033.
- [4] LHCb Collaboration, R. Aaij, et al., Measurement of the CKM angle γ from a combination of $B \rightarrow Dh$ analyses, Phys. Lett. B 726 (2013) 151, arXiv: 1305.2050.
- [5] R. Aleksov, I. Dunietz, B. Kayser, Determining the CP violating phase γ , Z. Phys. C 54 (1992) 653.
- [6] R. Fleischer, New strategies to obtain insights into CP violation through $B_s^0 \rightarrow D_s^\pm K^\mp$, $D_s^\pm K^\mp$, and $B_d^0 \rightarrow D^\pm \pi^\mp$, $D^{*\pm} \pi^\mp$ decays, Nucl. Phys. B 671 (2003) 459, arXiv:hep-ph/0304027.
- [7] M. Gronau, D. London, How to determine all the angles of the unitarity triangle from $B^0 \rightarrow DK_S$ and $B_s^0 \rightarrow D\phi$, Phys. Lett. B 253 (1991) 483.
- [8] LHCb Collaboration, R. Aaij, et al., Determination of the sign of the decay width difference in the B_s system, Phys. Rev. Lett. 108 (2012) 241801, arXiv: 1202.4717.
- [9] M. Gronau, et al., Using untagged $B^0 \rightarrow DK_S^0$ to determine γ , Phys. Rev. D 69 (2004) 113003, arXiv:hep-ph/0402055.
- [10] M. Gronau, Y. Grossman, Z. Surujon, J. Zupan, Enhanced effects on extracting γ from untagged B^0 and B_s^0 decays, Phys. Lett. B 649 (2007) 61, arXiv:hep-ph/0702011.
- [11] S. Ricciardi, Measuring the CKM angle γ at LHCb using untagged $B_s^0 \rightarrow D\phi$ decays, CERN-LHCb-PUB-2010-005.
- [12] LHCb Collaboration, R. Aaij, et al., First observation of the decay $\bar{B}_s^0 \rightarrow D^0 K^{*0}$ and a measurement of the ratio of branching fractions $\frac{\mathcal{B}(\bar{B}_s^0 \rightarrow D^0 K^{*0})}{\mathcal{B}(B^0 \rightarrow D^0 \rho^0)}$, Phys. Lett. B 706 (2011) 32, arXiv:1110.3676.
- [13] LHCb Collaboration, A.A. Alves Jr., et al., The LHCb detector at the LHC, J. Instrum. 3 (2008) S08005.
- [14] M. Adinolfi, et al., Performance of the LHCb RICH detector at the LHC, Eur. Phys. J. C 73 (2013) 2431, arXiv:1211.6759.
- [15] A.A. Alves Jr., et al., Performance of the LHCb muon system, J. Instrum. 8 (2010) P02022, arXiv:1211.1346.
- [16] R. Aaij, et al., The LHCb trigger and its performance in 2011, J. Instrum. 8 (2013) P04022, arXiv:1211.3055.
- [17] T. Sjöstrand, S. Mrenna, P. Skands, PYTHIA 6.4 physics and manual, J. High Energy Phys. 0605 (2006) 026, arXiv:hep-ph/0603175.
- [18] I. Belyaev, et al., Handling of the generation of primary events in Gauss, the LHCb simulation framework, Nucl. Sci. Symposium Conf. Record (NSS/MIC) IEEE (2010) 1155.
- [19] D.J. Lange, The EvtGen particle decay simulation package, Nucl. Instrum. Methods A 462 (2001) 152.
- [20] P. Golonka, Z. Was, PHOTOS Monte Carlo: a precision tool for QED corrections in Z and W decays, Eur. Phys. J. C 45 (2006) 97, arXiv:hep-ph/0506026.
- [21] Geant4 Collaboration, J. Allison, et al., Geant4 developments and applications, IEEE Trans. Nucl. Sci. 53 (2006) 270;
Geant4 Collaboration, S. Agostinelli, et al., Geant4: a simulation toolkit, Nucl. Instrum. Methods A 506 (2003) 250.
- [22] M. Clemencic, et al., The LHCb simulation application, GAUSS: design, evolution and experience, J. Phys. Conf. Ser. 331 (2011) 032023.
- [23] Particle Data Group, J. Beringer, et al., Review of particle physics, Phys. Rev. D 86 (2012) 010001, and 2013 partial update for the 2014 edition.
- [24] LHCb Collaboration, R. Aaij, et al., Observation of the decay $B^0 \rightarrow \bar{D}^0 K^+ K^-$ and evidence of $B_s^0 \rightarrow \bar{D}^0 K^+ K^-$, Phys. Rev. Lett. 109 (2012) 131801, arXiv: 1207.5991.
- [25] LHCb Collaboration, R. Aaij, et al., Measurement of the branching fractions of the decays $B_s^0 \rightarrow \bar{D}^0 K^- \pi^+$ and $B^0 \rightarrow \bar{D}^0 K^+ \pi^-$, Phys. Rev. D 87 (2013) 112009, arXiv:1304.6317.
- [26] L. Breiman, J.H. Friedman, R.A. Olshen, C.J. Stone, Classification and regression trees, Wadsworth International Group, Belmont, California, USA, 1984.
- [27] T. Skwarnicki, A study of the radiative cascade transitions between the Upsilon-prime and Upsilon resonances, PhD thesis, Institute of Nuclear Physics, Krakow, 1986, DESY-F31-86-02.
- [28] K.S. Cranmer, Kernel estimation in high-energy physics, Comput. Phys. Commun. 136 (2001) 198, arXiv:hep-ex/0011057.
- [29] M. Pivk, F.R. Le Diberder, sPlot: a statistical tool to unfold data distributions, Nucl. Instrum. Methods A 555 (2005) 356, arXiv:physics/0402083.
- [30] D. Aston, et al., A study of $K^- \pi^+$ scattering in the reaction $K^- p \rightarrow K^- \pi^+ n$ at 11 GeV/c, Nucl. Phys. B 296 (1988) 493;
BaBar Collaboration, B. Aubert, et al., Time-dependent and time-integrated angular analysis of $B \rightarrow \phi K_S^0 \pi^0$ and $\phi K^\pm \pi^\mp$, Phys. Rev. D 78 (2008) 092008, arXiv:0808.3586.
- [31] LHCb Collaboration, R. Aaij, et al., Measurement of the fragmentation fraction ratio f_s/f_d and its dependence on B meson kinematics, J. High Energy Phys. 1304 (2013) 001, arXiv:1301.5286.

LHCb Collaboration

R. Aaij⁴⁰, B. Adeva³⁶, M. Adinolfi⁴⁵, C. Adrover⁶, A. Affolder⁵¹, Z. Ajaltouni⁵, J. Albrecht⁹, F. Alessio³⁷, M. Alexander⁵⁰, S. Ali⁴⁰, G. Alkhazov²⁹, P. Alvarez Cartelle³⁶, A.A. Alves Jr.^{24,37}, S. Amato², S. Amerio²¹, Y. Amhis⁷, L. Anderlini^{17,f}, J. Anderson³⁹, R. Andreassen⁵⁶, J.E. Andrews⁵⁷, R.B. Appleby⁵³, O. Aquines Gutierrez¹⁰, F. Archilli¹⁸, A. Artamonov³⁴, M. Artuso⁵⁸, E. Aslanides⁶, G. Auriemma^{24,m}, M. Baalouch⁵, S. Bachmann¹¹, J.J. Back⁴⁷, C. Baesso^{59,t}, V. Balagura³⁰, W. Baldini¹⁶, R.J. Barlow⁵³, C. Barschel³⁷, S. Barsuk⁷, W. Barter⁴⁶, Th. Bauer⁴⁰, A. Bay³⁸, J. Beddow⁵⁰, F. Bedeschi²², I. Bediaga¹, S. Belogurov³⁰, K. Belous³⁴, I. Belyaev³⁰, E. Ben-Haim⁸, G. Bencivenni¹⁸, S. Benson⁴⁹, J. Benton⁴⁵, A. Berezhnoy³¹, R. Bernet³⁹, M.-O. Bettler⁴⁶, M. van Beuzekom⁴⁰, A. Bien¹¹, S. Bifani⁴⁴, T. Bird⁵³, A. Bizzeti^{17,h}, P.M. Bjørnstad⁵³, T. Blake³⁷, F. Blanc³⁸, J. Blouw¹¹, S. Blusk⁵⁸, V. Bocci²⁴, A. Bondar³³, N. Bondar²⁹, W. Bonivento¹⁵, S. Borghi⁵³, A. Borgia⁵⁸, T.J.V. Bowcock⁵¹, E. Bowen³⁹, C. Bozzi¹⁶, T. Brambach⁹, J. van den Brand⁴¹, J. Bressieux³⁸, D. Brett⁵³, M. Britsch¹⁰, T. Britton⁵⁸, N.H. Brook⁴⁵, H. Brown⁵¹, I. Burducea²⁸, A. Bursche³⁹, G. Busetto^{21,q}, J. Buytaert³⁷, S. Cadeddu¹⁵, O. Callot⁷, M. Calvi^{20,j}, M. Calvo Gomez^{35,n}, A. Camboni³⁵, P. Campana^{18,37}, D. Campora Perez³⁷, A. Carbone^{14,c}, G. Carboni^{23,k}, R. Cardinale^{19,i}, A. Cardini¹⁵, H. Carranza-Mejia⁴⁹, L. Carson⁵², K. Carvalho Akiba², G. Casse⁵¹, L. Castillo Garcia³⁷, M. Cattaneo³⁷, Ch. Cauet⁹, R. Cenci⁵⁷, M. Charles⁵⁴, Ph. Charpentier³⁷, P. Chen^{3,38}, N. Chiapolini³⁹, M. Chrzaszcz²⁵, K. Ciba³⁷, X. Cid Vidal³⁷, G. Ciezarek⁵², P.E.L. Clarke⁴⁹, M. Clemencic³⁷, H.V. Cliff⁴⁶, J. Closier³⁷, C. Coca²⁸, V. Coco⁴⁰, J. Cogan⁶, E. Cogneras⁵, P. Collins³⁷, A. Comerma-Montells³⁵, A. Contu^{15,37}, A. Cook⁴⁵, M. Coombes⁴⁵, S. Coquereau⁸, G. Corti³⁷,

- B. Couturier ³⁷, G.A. Cowan ⁴⁹, D.C. Craik ⁴⁷, S. Cunliffe ⁵², R. Currie ⁴⁹, C. D'Ambrosio ³⁷, P. David ⁸, P.N.Y. David ⁴⁰, A. Davis ⁵⁶, I. De Bonis ⁴, K. De Bruyn ⁴⁰, S. De Capua ⁵³, M. De Cian ¹¹, J.M. De Miranda ¹, L. De Paula ², W. De Silva ⁵⁶, P. De Simone ¹⁸, D. Decamp ⁴, M. Deckenhoff ⁹, L. Del Buono ⁸, N. Déléage ⁴, D. Derkach ⁵⁴, O. Deschamps ⁵, F. Dettori ⁴¹, A. Di Canto ¹¹, H. Dijkstra ³⁷, M. Dogaru ²⁸, S. Donleavy ⁵¹, F. Dordei ¹¹, A. Dosil Suárez ³⁶, D. Dossett ⁴⁷, A. Dovbnya ⁴², F. Dupertuis ³⁸, P. Durante ³⁷, R. Dzhelyadin ³⁴, A. Dziurda ²⁵, A. Dzyuba ²⁹, S. Easo ⁴⁸, U. Egede ⁵², V. Egorychev ³⁰, S. Eidelman ³³, D. van Eijk ⁴⁰, S. Eisenhardt ⁴⁹, U. Eitschberger ⁹, R. Ekelhof ⁹, L. Eklund ^{50,37}, I. El Rifai ⁵, Ch. Elsasser ³⁹, A. Falabella ^{14,e}, C. Färber ¹¹, G. Fardell ⁴⁹, C. Farinelli ⁴⁰, S. Farry ⁵¹, D. Ferguson ⁴⁹, V. Fernandez Albor ³⁶, F. Ferreira Rodrigues ¹, M. Ferro-Luzzi ³⁷, S. Filippov ³², M. Fiore ¹⁶, C. Fitzpatrick ³⁷, M. Fontana ¹⁰, F. Fontanelli ^{19,i}, R. Forty ³⁷, O. Francisco ², M. Frank ³⁷, C. Frei ³⁷, M. Frosini ^{17,f}, S. Furcas ²⁰, E. Furfarò ^{23,k}, A. Gallas Torreira ³⁶, D. Galli ^{14,c}, M. Gandelman ², P. Gandini ⁵⁸, Y. Gao ³, J. Garofoli ⁵⁸, P. Garosi ⁵³, J. Garra Tico ⁴⁶, L. Garrido ³⁵, C. Gaspar ³⁷, R. Gauld ⁵⁴, E. Gersabeck ¹¹, M. Gersabeck ⁵³, T. Gershon ^{47,37}, Ph. Ghez ⁴, V. Gibson ⁴⁶, L. Giubega ²⁸, V.V. Gligorov ³⁷, C. Göbel ^{59,t}, D. Golubkov ³⁰, A. Golutvin ^{52,30,37}, A. Gomes ², P. Gorbounov ^{30,37}, H. Gordon ³⁷, C. Gotti ²⁰, M. Grabalosa Gándara ⁵, R. Graciani Diaz ³⁵, L.A. Granado Cardoso ³⁷, E. Graugés ³⁵, G. Graziani ¹⁷, A. Grecu ²⁸, E. Greening ⁵⁴, S. Gregson ⁴⁶, P. Griffith ⁴⁴, O. Grünberg ^{60,u}, B. Gui ⁵⁸, E. Gushchin ³², Yu. Guz ^{34,37}, T. Gys ³⁷, C. Hadjivasiliou ⁵⁸, G. Haefeli ³⁸, C. Haen ³⁷, S.C. Haines ⁴⁶, S. Hall ⁵², B. Hamilton ⁵⁷, T. Hampson ⁴⁵, S. Hansmann-Menzemer ¹¹, N. Harnew ⁵⁴, S.T. Harnew ⁴⁵, J. Harrison ⁵³, T. Hartmann ^{60,u}, J. He ³⁷, T. Head ³⁷, V. Heijne ⁴⁰, K. Hennessy ⁵¹, P. Henrard ⁵, J.A. Hernando Morata ³⁶, E. van Herwijnen ³⁷, M. Hess ^{60,u}, A. Hicheur ¹, E. Hicks ⁵¹, D. Hill ⁵⁴, M. Hoballah ⁵, C. Hombach ⁵³, P. Hopchev ⁴, W. Hulsbergen ⁴⁰, P. Hunt ⁵⁴, T. Huse ⁵¹, N. Hussain ⁵⁴, D. Hutchcroft ⁵¹, D. Hynds ⁵⁰, V. Iakovenko ⁴³, M. Idzik ²⁶, P. Ilten ¹², R. Jacobsson ³⁷, A. Jaeger ¹¹, E. Jans ⁴⁰, P. Jaton ³⁸, A. Jawahery ⁵⁷, F. Jing ³, M. John ⁵⁴, D. Johnson ⁵⁴, C.R. Jones ⁴⁶, C. Joram ³⁷, B. Jost ³⁷, M. Kaballo ⁹, S. Kandybei ⁴², W. Kanso ⁶, M. Karacson ³⁷, T.M. Karbach ³⁷, I.R. Kenyon ⁴⁴, T. Ketel ⁴¹, A. Keune ³⁸, B. Khanji ²⁰, O. Kochebina ⁷, I. Komarov ³⁸, R.F. Koopman ⁴¹, P. Koppenburg ⁴⁰, M. Korolev ³¹, A. Kozlinskiy ⁴⁰, L. Kravchuk ³², K. Kreplin ¹¹, M. Kreps ⁴⁷, G. Krocker ¹¹, P. Krokovny ³³, F. Kruse ⁹, M. Kucharczyk ^{20,25,j}, V. Kudryavtsev ³³, T. Kvaratskheliya ^{30,37}, V.N. La Thi ³⁸, D. Lacarrere ³⁷, G. Lafferty ⁵³, A. Lai ¹⁵, D. Lambert ⁴⁹, R.W. Lambert ⁴¹, E. Lanciotti ³⁷, G. Lanfranchi ¹⁸, C. Langenbruch ³⁷, T. Latham ⁴⁷, C. Lazzeroni ⁴⁴, R. Le Gac ⁶, J. van Leerdam ⁴⁰, J.-P. Lees ⁴, R. Lefèvre ⁵, A. Leflat ³¹, J. Lefrançois ⁷, S. Leo ²², O. Leroy ⁶, T. Lesiak ²⁵, B. Leverington ¹¹, Y. Li ³, L. Li Gioi ⁵, M. Liles ⁵¹, R. Lindner ³⁷, C. Linn ¹¹, B. Liu ³, G. Liu ³⁷, S. Lohn ³⁷, I. Longstaff ⁵⁰, J.H. Lopes ², N. Lopez-March ³⁸, H. Lu ³, D. Lucchesi ^{21,q}, J. Luisier ³⁸, H. Luo ⁴⁹, F. Machefert ⁷, I.V. Machikhiliyan ^{4,30}, F. Maciuc ²⁸, O. Maev ^{29,37}, S. Malde ⁵⁴, G. Manca ^{15,d}, G. Mancinelli ⁶, J. Maratas ⁵, U. Marconi ¹⁴, P. Marino ^{22,s}, R. Märki ³⁸, J. Marks ¹¹, G. Martellotti ²⁴, A. Martens ⁸, A. Martín Sánchez ⁷, M. Martinelli ⁴⁰, D. Martinez Santos ⁴¹, D. Martins Tostes ², A. Martynov ³¹, A. Massafferri ¹, R. Matev ³⁷, Z. Mathe ³⁷, C. Matteuzzi ²⁰, E. Maurice ⁶, A. Mazurov ^{16,32,37,e}, J. McCarthy ⁴⁴, A. McNab ⁵³, R. McNulty ¹², B. McSkelly ⁵¹, B. Meadows ^{56,54}, F. Meier ⁹, M. Meissner ¹¹, M. Merk ⁴⁰, D.A. Milanes ⁸, M.-N. Minard ⁴, J. Molina Rodriguez ^{59,t}, S. Monteil ⁵, D. Moran ⁵³, P. Morawski ²⁵, A. Mordà ⁶, M.J. Morello ^{22,s}, R. Mountain ⁵⁸, I. Mous ⁴⁰, F. Muheim ⁴⁹, K. Müller ³⁹, R. Muresan ²⁸, B. Muryn ²⁶, B. Muster ³⁸, P. Naik ⁴⁵, T. Nakada ³⁸, R. Nandakumar ⁴⁸, I. Nasteva ¹, M. Needham ⁴⁹, S. Neubert ³⁷, N. Neufeld ³⁷, A.D. Nguyen ³⁸, T.D. Nguyen ³⁸, C. Nguyen-Mau ^{38,o}, M. Nicol ⁷, V. Niess ⁵, R. Niet ⁹, N. Nikitin ³¹, T. Nikodem ¹¹, A. Nomerotski ⁵⁴, A. Novoselov ³⁴, A. Oblakowska-Mucha ²⁶, V. Obraztsov ³⁴, S. Oggero ⁴⁰, S. Ogilvy ⁵⁰, O. Okhrimenko ⁴³, R. Oldeman ^{15,d}, M. Orlandea ²⁸, J.M. Otalora Goicochea ², P. Owen ⁵², A. Oyanguren ³⁵, B.K. Pal ⁵⁸, A. Palano ^{13,b}, T. Palczewski ²⁷, M. Palutan ¹⁸, J. Panman ³⁷, A. Papanestis ⁴⁸, M. Pappagallo ⁵⁰, C. Parkes ⁵³, C.J. Parkinson ⁵², G. Passaleva ¹⁷, G.D. Patel ⁵¹, M. Patel ⁵², G.N. Patrick ⁴⁸, C. Patrignani ^{19,i}, C. Pavel-Nicorescu ²⁸, A. Pazos Alvarez ³⁶, A. Pellegrino ⁴⁰, G. Penso ^{24,l}, M. Pepe Altarelli ³⁷, S. Perazzini ^{14,c}, E. Perez Trigo ³⁶, A. Pérez-Calero Yzquierdo ³⁵, P. Perret ⁵, M. Perrin-Terrin ⁶, L. Pescatore ⁴⁴, E. Pesen ^{61,v}, K. Petridis ⁵², A. Petrolini ^{19,i}, A. Phan ⁵⁸, E. Picatoste Olloqui ³⁵, B. Pietrzyk ⁴, T. Pilarčík ⁴⁷, D. Pinci ²⁴, S. Playfer ⁴⁹, M. Plo Casasus ³⁶, F. Polci ⁸, G. Polok ²⁵, A. Poluektov ^{47,33}, E. Polycarpo ², A. Popov ³⁴, D. Popov ¹⁰, B. Popovici ²⁸, C. Potterat ³⁵, A. Powell ⁵⁴, J. Prisciandaro ³⁸, A. Pritchard ⁵¹, C. Prouve ⁷, V. Pugatch ⁴³, A. Puig Navarro ³⁸, G. Punzi ^{22,r}, W. Qian ⁴, J.H. Rademacker ⁴⁵, B. Rakotomiaramanana ³⁸, M.S. Rangel ², I. Raniuk ⁴², N. Rauschmayr ³⁷, G. Raven ⁴¹, S. Redford ⁵⁴,

M.M. Reid ⁴⁷, A.C. dos Reis ¹, S. Ricciardi ^{48,*}, A. Richards ⁵², K. Rinnert ⁵¹, V. Rives Molina ³⁵,
 D.A. Roa Romero ⁵, P. Robbe ⁷, D.A. Roberts ⁵⁷, E. Rodrigues ⁵³, P. Rodriguez Perez ³⁶, S. Roiser ³⁷,
 V. Romanovsky ³⁴, A. Romero Vidal ³⁶, J. Rouvinet ³⁸, T. Ruf ³⁷, F. Ruffini ²², H. Ruiz ³⁵, P. Ruiz Valls ³⁵,
 G. Sabatino ^{24,k}, J.J. Saborido Silva ³⁶, N. Sagidova ²⁹, P. Sail ⁵⁰, B. Saitta ^{15,d}, V. Salustino Guimaraes ²,
 B. Sanmartin Sedes ³⁶, M. Sannino ^{19,i}, R. Santacesaria ²⁴, C. Santamarina Rios ³⁶, E. Santovetti ^{23,k},
 M. Sapunov ⁶, A. Sarti ^{18,l}, C. Satriano ^{24,m}, A. Satta ²³, M. Savrie ^{16,e}, D. Savrina ^{30,31}, P. Schaack ⁵²,
 M. Schiller ⁴¹, H. Schindler ³⁷, M. Schlupp ⁹, M. Schmelling ¹⁰, B. Schmidt ³⁷, O. Schneider ³⁸,
 A. Schopper ³⁷, M.-H. Schune ⁷, R. Schwemmer ³⁷, B. Sciascia ¹⁸, A. Sciubba ²⁴, M. Seco ³⁶,
 A. Semennikov ³⁰, K. Senderowska ²⁶, I. Sepp ⁵², N. Serra ³⁹, J. Serrano ⁶, P. Seyfert ¹¹, M. Shapkin ³⁴,
 I. Shapoval ^{16,42}, P. Shatalov ³⁰, Y. Shcheglov ²⁹, T. Shears ^{51,37}, L. Shekhtman ³³, O. Shevchenko ⁴²,
 V. Shevchenko ³⁰, A. Shires ⁹, R. Silva Coutinho ⁴⁷, M. Sirendi ⁴⁶, N. Skidmore ⁴⁵, T. Skwarnicki ⁵⁸,
 N.A. Smith ⁵¹, E. Smith ^{54,48}, J. Smith ⁴⁶, M. Smith ⁵³, M.D. Sokoloff ⁵⁶, F.J.P. Soler ⁵⁰, F. Soomro ¹⁸,
 D. Souza ⁴⁵, B. Souza De Paula ², B. Spaan ⁹, A. Sparkes ⁴⁹, P. Spradlin ⁵⁰, F. Stagni ³⁷, S. Stahl ¹¹,
 O. Steinkamp ³⁹, S. Stevenson ⁵⁴, S. Stoica ²⁸, S. Stone ⁵⁸, B. Storaci ³⁹, M. Straticiuc ²⁸, U. Straumann ³⁹,
 V.K. Subbiah ³⁷, L. Sun ⁵⁶, S. Swientek ⁹, V. Syropoulos ⁴¹, M. Szczekowski ²⁷, P. Szczypka ^{38,37},
 T. Szumlak ²⁶, S. T'Jampens ⁴, M. Teklichyn ⁷, E. Teodorescu ²⁸, F. Teubert ³⁷, C. Thomas ⁵⁴, E. Thomas ³⁷,
 J. van Tilburg ¹¹, V. Tisserand ⁴, M. Tobin ³⁸, S. Tolk ⁴¹, D. Tonelli ³⁷, S. Topp-Joergensen ⁵⁴, N. Torr ⁵⁴,
 E. Tournefier ^{4,52}, S. Tourneur ³⁸, M.T. Tran ³⁸, M. Tresch ³⁹, A. Tsaregorodtsev ⁶, P. Tsopelas ⁴⁰,
 N. Tuning ⁴⁰, M. Ubeda Garcia ³⁷, A. Ukleja ²⁷, D. Urner ⁵³, A. Ustyuzhanin ^{52,p}, U. Uwer ¹¹, V. Vagnoni ¹⁴,
 G. Valenti ¹⁴, A. Vallier ⁷, M. Van Dijk ⁴⁵, R. Vazquez Gomez ¹⁸, P. Vazquez Regueiro ³⁶,
 C. Vázquez Sierra ³⁶, S. Vecchi ¹⁶, J.J. Velthuis ⁴⁵, M. Veltri ^{17,g}, G. Veneziano ³⁸, M. Vesterinen ³⁷,
 B. Viaud ⁷, D. Vieira ², X. Vilasis-Cardona ^{35,n}, A. Vollhardt ³⁹, D. Volyansky ¹⁰, D. Voong ⁴⁵,
 A. Vorobyev ²⁹, V. Vorobyev ³³, C. Voß ^{60,u}, H. Voss ¹⁰, R. Waldi ^{60,u}, C. Wallace ⁴⁷, R. Wallace ¹²,
 S. Wandernoth ¹¹, J. Wang ⁵⁸, D.R. Ward ⁴⁶, N.K. Watson ⁴⁴, A.D. Webber ⁵³, D. Websdale ⁵²,
 M. Whitehead ⁴⁷, J. Wicht ³⁷, J. Wiechczynski ²⁵, D. Wiedner ¹¹, L. Wiggers ⁴⁰, G. Wilkinson ⁵⁴,
 M.P. Williams ^{47,48}, M. Williams ⁵⁵, F.F. Wilson ⁴⁸, J. Wimberley ⁵⁷, J. Wishahi ⁹, W. Wislicki ²⁷,
 M. Witek ²⁵, S.A. Wotton ⁴⁶, S. Wright ⁴⁶, S. Wu ³, K. Wyllie ³⁷, Y. Xie ^{49,37}, Z. Xing ⁵⁸, Z. Yang ³,
 R. Young ⁴⁹, X. Yuan ³, O. Yushchenko ³⁴, M. Zangoli ¹⁴, M. Zavertyaev ^{10,a}, F. Zhang ³, L. Zhang ⁵⁸,
 W.C. Zhang ¹², Y. Zhang ³, A. Zhelezov ¹¹, A. Zhokhov ³⁰, L. Zhong ³, A. Zvyagin ³⁷

¹ Centro Brasileiro de Pesquisas Físicas (CBPF), Rio de Janeiro, Brazil² Universidade Federal do Rio de Janeiro (UFRJ), Rio de Janeiro, Brazil³ Center for High Energy Physics, Tsinghua University, Beijing, China⁴ LAPP, Université de Savoie, CNRS/IN2P3, Annecy-Le-Vieux, France⁵ Clermont Université, Université Blaise Pascal, CNRS/IN2P3, LPC, Clermont-Ferrand, France⁶ CPPM, Aix-Marseille Université, CNRS/IN2P3, Marseille, France⁷ LAL, Université Paris-Sud, CNRS/IN2P3, Orsay, France⁸ LPNHE, Université Pierre et Marie Curie, Université Paris Diderot, CNRS/IN2P3, Paris, France⁹ Fakultät Physik, Technische Universität Dortmund, Dortmund, Germany¹⁰ Max-Planck-Institut für Kernphysik (MPIK), Heidelberg, Germany¹¹ Physikalisches Institut, Ruprecht-Karls-Universität Heidelberg, Heidelberg, Germany¹² School of Physics, University College Dublin, Dublin, Ireland¹³ Sezione INFN di Bari, Bari, Italy¹⁴ Sezione INFN di Bologna, Bologna, Italy¹⁵ Sezione INFN di Cagliari, Cagliari, Italy¹⁶ Sezione INFN di Ferrara, Ferrara, Italy¹⁷ Sezione INFN di Firenze, Firenze, Italy¹⁸ Laboratori Nazionali dell'INFN di Frascati, Frascati, Italy¹⁹ Sezione INFN di Genova, Genova, Italy²⁰ Sezione INFN di Milano Bicocca, Milano, Italy²¹ Sezione INFN di Padova, Padova, Italy²² Sezione INFN di Pisa, Pisa, Italy²³ Sezione INFN di Roma Tor Vergata, Roma, Italy²⁴ Sezione INFN di Roma La Sapienza, Roma, Italy²⁵ Henryk Niewodniczanski Institute of Nuclear Physics, Polish Academy of Sciences, Kraków, Poland²⁶ AGH – University of Science and Technology, Faculty of Physics and Applied Computer Science, Kraków, Poland²⁷ National Center for Nuclear Research (NCBJ), Warsaw, Poland²⁸ Horia Hulubei National Institute of Physics and Nuclear Engineering, Bucharest-Magurele, Romania²⁹ Petersburg Nuclear Physics Institute (PNPI), Gatchina, Russia³⁰ Institute of Theoretical and Experimental Physics (ITEP), Moscow, Russia³¹ Institute of Nuclear Physics, Moscow State University (SINP MSU), Moscow, Russia³² Institute for Nuclear Research of the Russian Academy of Sciences (INR RAN), Moscow, Russia³³ Budker Institute of Nuclear Physics (SB RAS) and Novosibirsk State University, Novosibirsk, Russia³⁴ Institute for High Energy Physics (IHEP), Protvino, Russia

- ³⁵ Universitat de Barcelona, Barcelona, Spain
³⁶ Universidad de Santiago de Compostela, Santiago de Compostela, Spain
³⁷ European Organization for Nuclear Research (CERN), Geneva, Switzerland
³⁸ Ecole Polytechnique Fédérale de Lausanne (EPFL), Lausanne, Switzerland
³⁹ Physik-Institut, Universität Zürich, Zürich, Switzerland
⁴⁰ Nikhef National Institute for Subatomic Physics, Amsterdam, The Netherlands
⁴¹ Nikhef National Institute for Subatomic Physics and VU University Amsterdam, Amsterdam, The Netherlands
⁴² NSC Kharkiv Institute of Physics and Technology (NSC KIPT), Kharkiv, Ukraine
⁴³ Institute for Nuclear Research of the National Academy of Sciences (KINR), Kyiv, Ukraine
⁴⁴ University of Birmingham, Birmingham, United Kingdom
⁴⁵ H.H. Wills Physics Laboratory, University of Bristol, Bristol, United Kingdom
⁴⁶ Cavendish Laboratory, University of Cambridge, Cambridge, United Kingdom
⁴⁷ Department of Physics, University of Warwick, Coventry, United Kingdom
⁴⁸ STFC Rutherford Appleton Laboratory, Didcot, United Kingdom
⁴⁹ School of Physics and Astronomy, University of Edinburgh, Edinburgh, United Kingdom
⁵⁰ School of Physics and Astronomy, University of Glasgow, Glasgow, United Kingdom
⁵¹ Oliver Lodge Laboratory, University of Liverpool, Liverpool, United Kingdom
⁵² Imperial College London, London, United Kingdom
⁵³ School of Physics and Astronomy, University of Manchester, Manchester, United Kingdom
⁵⁴ Department of Physics, University of Oxford, Oxford, United Kingdom
⁵⁵ Massachusetts Institute of Technology, Cambridge, MA, United States
⁵⁶ University of Cincinnati, Cincinnati, OH, United States
⁵⁷ University of Maryland, College Park, MD, United States
⁵⁸ Syracuse University, Syracuse, NY, United States
⁵⁹ Pontifícia Universidade Católica do Rio de Janeiro (PUC-Rio), Rio de Janeiro, Brazil ^t
⁶⁰ Institut für Physik, Universität Rostock, Rostock, Germany ^u
⁶¹ Celal Bayar University, Manisa, Turkey ^v

* Corresponding author.

^a P.N. Lebedev Physical Institute, Russian Academy of Science (LPI RAS), Moscow, Russia.

^b Università di Bari, Bari, Italy.

^c Università di Bologna, Bologna, Italy.

^d Università di Cagliari, Cagliari, Italy.

^e Università di Ferrara, Ferrara, Italy.

^f Università di Firenze, Firenze, Italy.

^g Università di Urbino, Urbino, Italy.

^h Università di Modena e Reggio Emilia, Modena, Italy.

ⁱ Università di Genova, Genova, Italy.

^j Università di Milano Bicocca, Milano, Italy.

^k Università di Roma Tor Vergata, Roma, Italy.

^l Università di Roma La Sapienza, Roma, Italy.

^m Università della Basilicata, Potenza, Italy.

ⁿ LIFAELS, La Salle, Universitat Ramon Llull, Barcelona, Spain.

^o Hanoi University of Science, Hanoi, Viet Nam.

^p Institute of Physics and Technology, Moscow, Russia.

^q Università di Padova, Padova, Italy.

^r Università di Pisa, Pisa, Italy.

^s Scuola Normale Superiore, Pisa, Italy.

^t Associated to Universidade Federal do Rio de Janeiro (UFRJ), Rio de Janeiro, Brazil.

^u Associated to Physikalisches Institut, Ruprecht-Karls-Universität Heidelberg, Heidelberg, Germany.

^v Associated to European Organization for Nuclear Research (CERN), Geneva, Switzerland.